S-wave attenuation caused by wave-induced fluid flow

Beatriz Quintal (ETH Zurich), Holger Steeb (Ruhr-University Bochum), Marcel Frehner (ETH Zurich), and Stefan M. Schmalholz (University of Lausanne)*

Summary

We study seismic wave attenuation ($1/Q$) caused by the physical mechanism of wave-induced fluid flow. Relaxation experiments are numerically performed to solve Biot's equations of consolidation. The experiments yield stress-strain relations used in a post-processing step to calculate the complex moduli of 2D poroelastic media with mesoscopic-scale heterogeneities. Attenuation is then determined from the complex moduli. In our model, the rock is represented by a medium containing circular heterogeneities of much lower porosity and permeability than the homogeneous background. The background contains 80% of the total pore space in the medium and is fully saturated with oil, gas, or water, while the heterogeneities are always fully saturated with water. We observe that the S-wave attenuation in the medium with 80% of oil is much higher than in the one with 80% of gas, and at low seismic frequencies (< 10 Hz), the S-wave attenuation in the medium with 80% of oil is also much higher than in the one with 100% of water. This occurs because the maximum value of the S-wave attenuation is shifted to lower frequencies with increasing fluid viscosity. Additionally, we observe that S-wave attenuation can be high (e.g., Q = 16) when the porous and permeable background has also a much more compliant solid frame than the low-porosity, low-permeability heterogeneities.

Introduction

Attenuation of seismic waves in partially saturated, porous rocks is of great interest because it has been observed that oil and gas reservoirs frequently exhibit high attenuation, especially at low seismic frequencies (Chapman et al., 2006). At low seismic frequencies, wave-induced fluid flow caused by fluid pressure differences between mesoscopic-scale heterogeneities is a major cause of P-wave attenuation in a partially saturated porous rock (e.g., White, 1975; Pride et al., 2004; Müller et al., 2010). The mesoscopic scale is the scale much larger than the pore size but much smaller than the wavelength. A partially saturated rock is approximated by a poroelastic medium with regions fully saturated by one fluid and other regions fully saturated by another fluid. This is frequently referred to as patchy saturation. Mesoscopic-scale heterogeneities can also occur in the porosity and other solid frame properties, taken into account by double-porosity models. In this paper, we study P- and S-wave attenuation in partially saturated rocks with a heterogeneous solid frame. We therefore introduce double porosity and patchy saturation in our models. We pay special attention to the S-wave attenuation. Because we consider commercial hydrocarbon reservoirs as the potential application of this study, we compare media with the following degrees of saturation: (1) 80% of oil, 20% of water; (2) 80% of gas, 20% of water; and (3) 100% of water.

Methodology

We use the finite element method to solve Biot's equations of consolidation (Biot, 1941) in the displacement-pressure (u-p) formulation (Zienkiewicz and Shiomi, 1984). We perform 2D quasi-static relaxation tests on poroelastic media with mesoscopic-scale heterogeneities to calculate the complex moduli from the modeled stress-strain relations. From the complex moduli, we calculate the frequency-dependent attenuation caused by fluid flow induced by pressure differences between regions of different compliances due to contrasts in fluid and/or solid frame properties. The numerical simulations are performed on the Representative Elementary Volume (REV) of the medium. The algorithm employs an unstructured mesh, shown in Figure 1, which makes it accurate for simulations in media with heterogeneities of arbitrary geometries. Additionally, it employs variable time stepping (red dots for $S(t)$ in Figure 4), which makes it very efficient. Small steps at the beginning are necessary to accurately resolve the high frequencies. For a detailed description of the algorithm, we refer to Quintal et al., (2011).

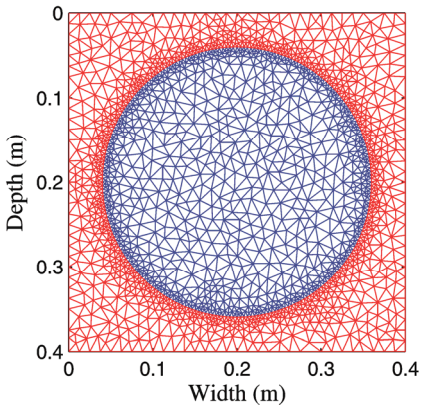

Figure 1. Unstructured finite element mesh of the REV with Delauney triangulation (Shewchuk, 2002). Each triangular element (quadratic-shape functions) consists of seven nodal points, on which the solid displacements and fluid pressure are calculated. Blue and red elements inside and outside the circular heterogeneity have different petrophysical properties. The spatial resolution of the mesh can strongly vary.

To calculate P- and S-wave attenuation, we model two relaxation experiments, a uniaxial pure compression test and a simple shear test, respectively (Figure 2). For the first, we attribute a time function $S(t)$ to the displacement in z-direction at the top boundary of the REV, and zero to the displacement in z-direction at the bottom and to the displacement in x-direction at the left and right boundaries. For the second experiment, simple shear is simulated by attributing $S(t)$ to the displacement in x-direction at the top and bottom boundaries of the REV, with opposite signs, and fixing the displacement in z-direction to zero in all the four boundaries. With the stress and strain rates obtained from the experiments, and converted to the frequency domain using a Fourier transform, we calculate the frequency-dependent, complex P-wave modulus, H,

$$H = \frac{\dot{\sigma}_{zz}}{\dot{\varepsilon}_{zz}}, \tag{1}$$

from the results of the uniaxial compression, and the frequency-dependent, complex undrained shear modulus, μ,

$$\mu = \frac{\dot{\sigma}_{xz}}{\dot{\varepsilon}_{xz}}, \tag{2}$$

using the results from the simple shear experiment. The symbols ε_{zz} and σ_{zz} represent the normal strain and total normal stress in z-direction, respectively, and ε_{xz} and σ_{xz} represent the shear strain and stress. The dot at the top of the symbols represents a partial time derivative. The complex and frequency-dependent moduli H and μ are used to calculate the P- and S-wave quality factors,

$$Q_P = \frac{\mathrm{Re}[H]}{\mathrm{Im}[H]}, \tag{3}$$

and

$$Q_S = \frac{\mathrm{Re}[\mu]}{\mathrm{Im}[\mu]}. \tag{4}$$

The inverse of quality factor is a measure of attenuation.

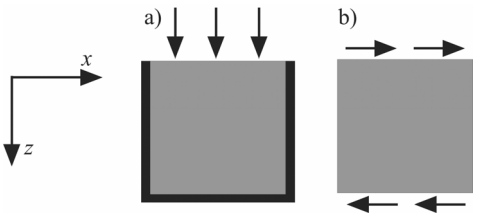

Figure 2. Sketch of the two relaxation experiments, uniaxial pure compression (a), and simple shear (b).

Simulations

Our main purpose is to evaluate fluid effects on P- and S-wave attenuation in rocks with a heterogeneous solid frame. The model consists of mesoscopic-scale circular heterogeneities characterized by low permeability and low porosity, embedded in a background medium of high permeability and high porosity. The REV is a 40-cm side square and the radius of the circular heterogeneity is 16 cm (Figure 1). The circle occupies 50% of the REV. Because of the different porosities of the heterogeneity and of the background (Table 2), the pore space in the background corresponds to 80% of the total pore space in the medium. The heterogeneities are always fully saturated with water, and the background is fully saturated with oil, gas, or water (Table 3). Three degrees of saturation are studied: (O) 80% of oil, 20% of water; (G) 80% of gas, 20% of water; and (W) 100% of water. The results for the real part of the P-wave modulus, H, the P-wave quality factor, Q_P, the real part of the undrained shear modulus, μ, and the S-wave quality factor, Q_S, are shown in Figure 3.

Table 1. Symbols.

ρ_s	Density of the grains
K_s	Bulk modulus of the grains
ϕ	Porosity
k	Permeability
K_d	Bulk modulus of the dry frame
μ_d	Shear modulus of the dry frame
ρ_f	Density of the fluid
η	Viscosity of the fluid
K_f	Bulk modulus of the fluid

Table 2. Physical properties of the solid frame.

Region	Heterogeneity	Background
ρ_s (kg/m^3)	2700	2700
K_s (GPa)	40	48
ϕ (%)	6	26
k (mD)	40	1000
K_d (GPa)	36	4
μ_d (GPa)	32	2

Table 3. Physical properties of the fluids.

Fluid	Water	Oil	Gas
ρ_f (kg/m^3)	1010	880	160
η (Pa s)	0.001	0.02	2×10^{-5}
K_f (GPa)	2.4	1.4	0.04

At the low-frequency (quasi-static) limit, our results (Figure 3) agree with the prediction of Gassmann's (1951) theory that the undrained shear modulus, μ, is independent on the properties of the saturating fluid. For higher frequencies, the value of μ changes with changing fluid saturation, which is predicted by Berryman and Wang (2001) by applying an effective-medium theory to poroelastic media consisting of a heterogeneous solid frame. Attenuation and velocity dispersion are implicit in the difference between their predictions for different frequency limits.

We observe in Figure 3 that both the P-wave attenuation ($1/Q_P$) and the S-wave attenuation ($1/Q_S$) are very low for

gas saturation. However, the S-wave attenuation is remarkably high at low frequencies for oil saturation. Although the minimum value of Q_S is lower for the fully water-saturated rock (10.4 at 64.6 Hz) than for the 80% oil-saturated one (15.8 at 4.4 Hz), at low frequencies (< 10 Hz), it is much lower in the 80% oil-saturated rock than in the fully water-saturated one (74 at 4.4 Hz).

The S-wave attenuation in this study is caused by fluid flow between the heterogeneity and the background, with different petrophysical properties. For the 80% oil-saturated rock, fluid flow between the water-saturated heterogeneity and the oil-saturated background is shown in Figure 4. Three stages of the simple shear relaxation experiment are shown for the fields ε_{xz} (shear strain), σ_{xz} (shear stress), P (pore fluid pressure), V_x (fluid velocity in the x-direction), and V_z (fluid velocity in the z-direction), all normalized by their respective maximum values. The displacements in x-direction, applied at top and bottom boundaries with different signs (Figure 2b), induce fluid pressure differences in the sample. These fluid pressure differences cause flow of the pore fluid, which is responsible for energy loss (i.e., attenuation).

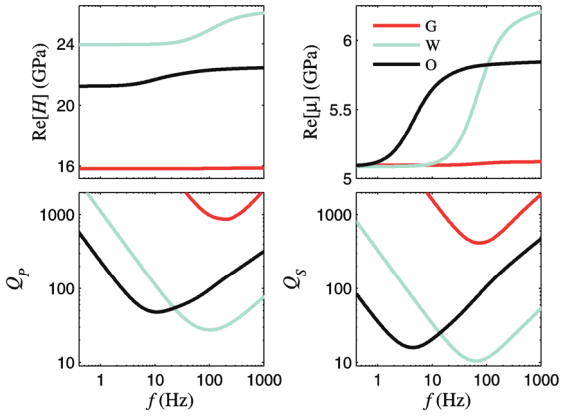

Figure 3. Numerical results for the real part of the P-wave modulus, H, the P-wave attenuation, $1/Q_P$, the real part of the undrained shear modulus, μ, and the S-wave attenuation, $1/Q_S$. The petrophysical parameters are given in Tables 2 and 3. The legend terms refer to the saturation in the numerical samples: 80% gas, 20% water (G); 100% water (W); and 80% oil, 20% water (O). In this order, at 4.4 Hz, the values of Q_S are 3520, 74.0, and 15.8.

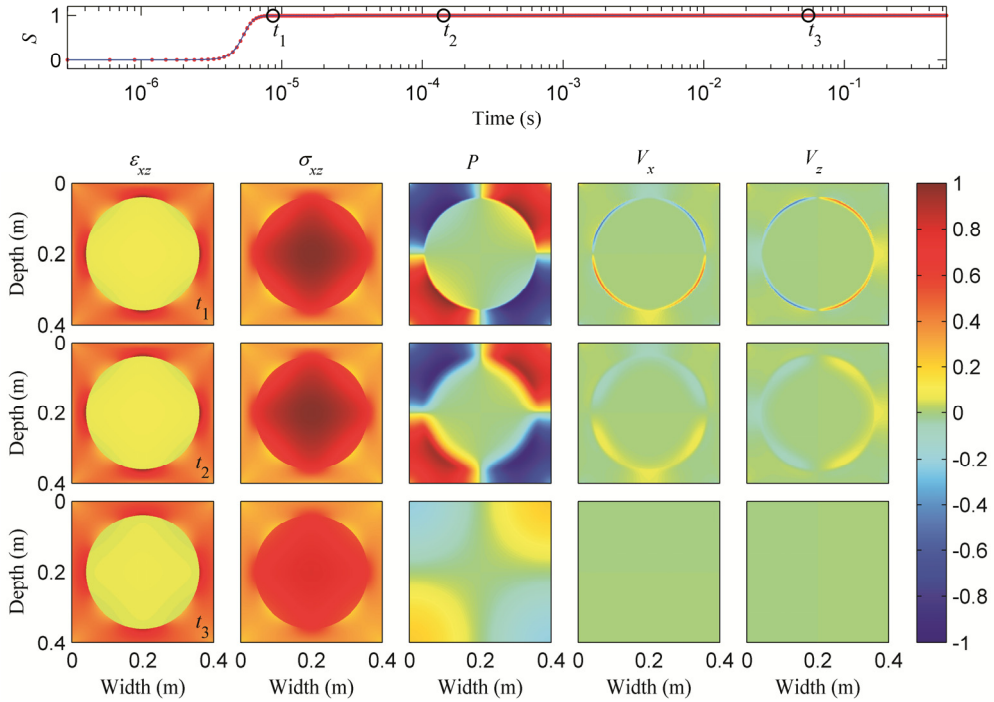

Figure 4. Three stages, t_1, t_2, and t_3, of the simple shear relaxation experiment (Figure 2b) on the REV for the sample with 80% oil saturation (water saturates the circular heterogeneity and oil saturates the more porous and permeable background). The results of this simulation for μ and Q_S are shown in Figure 3. In the top graph, the evolution of the boundary conditions, $S(t)$, normalized by its maximum value, is shown on a logarithmic time axis. For each stage, the fields ε_{xz} (shear strain), σ_{xz} (shear stress), P (pore fluid pressure), V_x (fluid velocity in the x-direction), and V_z (fluid velocity in the z-direction) are displayed, all normalized by their respective maximum values.

We also perform relaxation experiments considering another heterogeneous model with the same REV, same saturation degrees and same fluid properties as in the previous example. The solid frame properties are also given in Table 2, except K_d and μ_d, which are 4 and 2 GPa, respectively, in the heterogeneity, and 36 and 32 GPa, respectively, in the background. In this case, the less porous and permeable area (the heterogeneity) has the most compliant solid frame, which is probably less realistic than in the previous example. The results are shown in Figure 5. We observe that the P-wave attenuation can be very high in the media with 80% oil or gas saturation, but it can be also significant in the medium with 100% water saturation. However, the S-wave attenuation in all media is much lower than the P-wave attenuation and also much lower than the S-wave attenuation in the previous example.

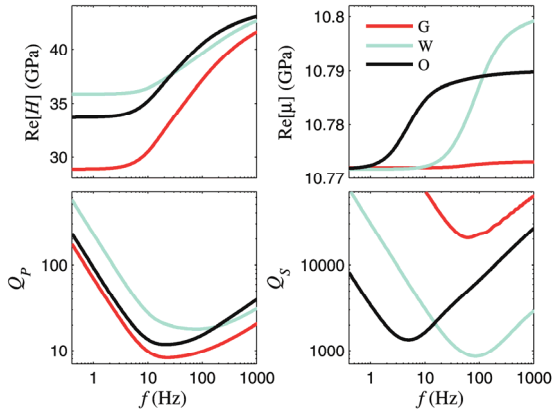

Figure 5. Numerical results for the real part of the P-wave modulus, H, the P-wave attenuation, $1/Q_P$, the real part of the undrained shear modulus, μ, and the S-wave attenuation, $1/Q_S$. The petrophysical parameters are the ones from Tables 2 and 3, except K_d and μ_d, which are 4 and 2 GPa, respectively, in the heterogeneity, and 36 and 32 GPa, respectively, in the background. So, for this figure, the less porous and permeable area (the heterogeneity) has the most compliant solid frame. The legend terms refer to the saturation in the sample: 80% gas, 20% water (G); 100% water (W); and 80% oil, 20% water (O).

In both Figures 3 and 5, the S-wave attenuation is much higher in the medium with 80% oil than in the one with 80% gas. Although the maximum values of S-wave attenuation in the media with 100% water are higher than the ones in the media with 80% oil, at frequencies below 10 Hz, the S-wave attenuation is significantly higher in the sample with 80% oil saturation in both figures. This occurs because, for very viscous fluids, the maximum value of S-wave attenuation is shifted to lower frequencies with increasing fluid viscosity.

Discussion and conclusions

It is well known that in White's model a medium of a homogeneous frame, partially (patchy) saturated with water and gas, exhibits high P-wave attenuation when it has a low gas saturation of around 10% (e.g., Quintal et al., 2009). However, when the medium has a heterogeneous frame, in addition to patchy saturation, more parameters rule the compressibility and fluid mobility (k/η) in the different regions, and the P-wave attenuation can be high for large oil or gas saturations, as shown in Figure 5.

We showed that the S-wave attenuation is much higher in a medium of heterogeneous solid frame when it is mostly saturated with oil than when it is mostly saturated with gas. In addition, at low seismic frequencies (< 10 Hz), the S-wave attenuation can be much higher in the medium mostly saturated with oil than in the one fully saturated with water. We also showed that when the more porous and permeable region has a much more compliant rock frame than the less porous and permeable region, the S-wave attenuation in the oil-saturated sample can be significantly high with, for example, $Q = 16$ (Figure 3).

Acknowledgements

This work has been supported by Spectraseis and the Low Frequency Seismic Partnership (LFSP). B. Quintal thanks Marc-André Lambert and Erik Saenger for helpful suggestions and discussions.

References

Berrymann, J. G., and H. F. Wang, 2001, Dispersion in poroelastic systems: Physical Review E, **64**, 011303.

Biot, M. A., 1941, General theory of three-dimensional consolidation: Journal of Applied Physics, **12**, 155-164.

Chapman, M., E. Liu, and X. Li, 2006, The influence of fluid-sensitive dispersion and attenuation on AVO analysis: Geophysical Journal International, **167**, 89-105.

Gassmann, F., 1951, Über die Elastizität poröser Medien: Vierteljahrsschrift der Naturforschenden Gesellschaft in Zürich, **96**, 1-23.

Müller, T. M., B. Gurevich, and M. Lebedev, 2010, Seismic wave attenuation and dispersion resulting from wave-induced flow in porous rocks – A review: Geophysics, **75**, A147-A164.

Pride, S. R., J. G. Berryman, and J. M. Harris, 2004, Seismic attenuation due to wave-induced flow: Journal of Geophysical Research, **109**, B01201.

Quintal, B., S. M. Schmalholz, and Y. Y. Podladchikov, 2009, Low-frequency reflections from a thin layer with high attenuation caused by interlayer flow: Geophysics, **74**, N15-N23.

Quintal, B., H. Steeb, M. Frehner, and S. M. Schmalholz, 2011, Quasi-static finite element modeling of seismic attenuation and dispersion due to wave-induced fluid flow in poroelastic media. Journal of Geophysical Research, **116**, B01201.

Shewchuk, J. R., 2002, Delaunay refinement algorithms for triangular mesh generation: Computational Geometry, **22**, 21-74.

White, J. E., 1975, Computed seismic speeds and attenuation in rocks with partial gas saturation: Geophysics, **40**, 224-232.

Zienkiewicz, O. C., and T. Shiomi, 1984, Dynamic behaviour of saturated porous media; the generalized Biot formulation and its numerical solution: International Journal for Numerical and Analytical Methods in Geomechanics, **8**, 71-96.